Cite this: DOI: 00.0000/xxxxxxxxxx

Structural relationships for the design of responsive azobenzene-based lyotropic liquid crystals†

Luke W. Giles,[a] Joshua B. Marlow,[a] Calum S. G. Butler,[a] Geosmin A. Turpin,[a] Liliana de Campo,[b] Stephen T. Mudie,[c] Charl F. J. Faul,[d] and Rico F. Tabor*[a]

Received Date
Accepted Date

DOI: 00.0000/xxxxxxxxxx

Light-responsive binary (azobenzene + solvent) lyotropic liquid crystals (LCs) were investigated by structural modification of simple azobenzene molecules. Three benzoic acid-containing azobenzene molecules 4-(4-(hydroxyphenyl)diazenyl)benzoic acid (AZO1), 3-(4-(hydroxyphenyl)diazenyl)benzoic acid (AZO2) and 5-(4-(hydroxyphenyl)diazenyl)isophthalic acid (AZO3) were produced with various amide substitutions to produce tectons with a variety of hydrophobicity, size and branching. The LC mesophases formed by binary (azobenzene + solvent) systems with low volatility solvents dimethylsulfoxide (DMSO) and *N,N*-dimethylformamide (DMF) as well as the protic ionic liquids ethylammonium formate (EAF) and propylammonium formate (PAF), were investigated using a combination of small-angle X-ray and neutron scattering (SAXS and SANS) as well as polarising light microscopy (PLM). Increasing alkyl group length was found to have a strong influence on LC phase spacing, and changes in the position of substitution on the benzene ring influenced the preferred curvature of phases. UV-induced *trans* to *cis* isomerization of the samples was shown to influence ordering and optical birefringence, indicating potential applications in optical devices.

1 Introduction

Liquid crystals (LCs) represent a state of matter that combines the short to mid-range order of crystalline solids with the flow properties of liquids.[1] The ability of LCs to align with surfaces and external electric fields, as well as the birefringence of many LC phases, has led to their application in devices such as displays,[2] sensors[3] and actuators.[4]

There are three main categories of liquid crystals: thermotropic, lyotropic and polymeric.[5] Thermotropic LCs change their aggregation state in response to changes in temperature, whereas lyotropic LCs, being multi-component systems, respond to changes in concentration and temperature. Polymeric LCs, or liquid crystal polymers, are materials often formed from block copolymers that exhibit ordering while maintaining the flow properties essential for liquid crystals.

Thermotropic liquid crystalline materials have been the most widely applied sub-class of liquid crystalline materials for optical and electro-optical application,[6] however, the need for thermal control of the systems means that the thermotropic liquid crystalline materials must have thermotropic phases at or close to room temperature for the majority of applications. Lyotropic liquid crystals offer the comparative advantage of both concentration and thermal control, allowing for facile manipulation of their properties and phase transitions to find a diverse array of readily accessible liquid crystalline phases.[7]

Stimuli-responsive materials are in high demand for the creation of "smart materials" that are able to change or modify their physical and/or chemical properties upon application of a stimulus.[8,9] Light is a particularly appealing choice of stimulus compared to other stimuli such as pH or temperature because it is non-invasive, generally non-harmful, spatiotemporally resolved and is comparatively low energy.[10–12] While LCs can be made to re-align to an external electric field, the introduction of light responsive behaviour is of interest for the creation of multi-responsive systems, non-linear optical materials,[13] optical gratings and filters,[14] responsive thin films[15–19] and holographic technology.[20]

One method for achieving such multi-responsive materials is the introduction of photochromic materials into the liquid crystal.[21–24] The azobenzene functional group is known to have a facile *E/Z* isomerization upon irradiation with UV light (Figure 1a). However, because of the propensity of azobenzenes to π-

[a] *School of Chemistry, Monash University, Clayton 3800, Victoria, Australia. Tel: (+61) 3 9905 4558; E-mail: rico.tabor@monash.edu*
[b] *Australian Centre for Neutron Scattering (ACNS), New Illawarra Road , Sydney, New South Wales, Australia.*
[c] *Australian Synchrotron, ANSTO, 800 Blackburn Rd, Clayton, 3168, Australia.*
[d] *School of Chemistry, University of Bristol, Cantock's Close, Bristol BS8 1TS, UK.*
† Electronic Supplementary Information (ESI) available: [details of any supplementary information available should be included here]. See DOI: 00.0000/00000000.

stack, unless specifically designed otherwise, azobenzene LC materials typically exhibit thermotropic liquid crystalline behaviour at temperatures higher than practical for industrial applications, with many reported melting points well above 100°C.[25–28] For this reason many investigations focus on doping other liquid crystalline systems with azobenzene chromophores.[13,15,20,28–30] Alternatively, lyotropic liquid crystals provide a potential remedy to this particular problem, while also allowing for the LC phases to have a greater proportion of azobenzene units in the LC formulation.

Recent endeavours towards the formation of azobenzene containing liquid crystals have included the the formation of commercial thermotropic liquid crystal mimics, such as 5CB mimics,[23] exploring a series of bromine terminated azobenzene molecules that formed smectic A (SmA) thermotropic liquid crystals. However, the observed LC transition temperatures, from 95-105°C, remain much greater than our room-temperature target. Other routes of investigation have included the incorporation of biologically relevant functional groups, such as chalcone and ester linkages[24] and bent molecule based liquid crystals, which have their own distinct self-assembled LC structures.[25,31] Zhu *et al.* performed a study introducing chalcone and ester linkages into a series of azobenzene molecules, however, the relevant thermotropic LC temperature transitions were found to be in excess of 110°C. Clearly this line of investigation could benefit from a better understanding of the driving forces for formation of lyotropic LC systems, which can occur at biologically relevant temperatures because of their similarity to biological structures such as cell membranes.

Despite the potential for the introduction of many and varied functionalities to conventional thermotropic liquid crystals, the induction of multi-dimensional changes in space group symmetry upon *trans* to *cis* isomerization remains a challenge. A recent study by Nagai *et al.* demonstrated the feasibility of such changes using an azobenzene photoswitch.[32] Their study found a ternary thermotropic system in which photo-isomerization was shown to induce transition between smectic C (SmC) and bicontinuous cubic ($Ia\bar{3}d$) spacegroups, however, this ternary system has a working temperature range around 400 K. Room temperature reproduction of such drastic space group changes therefore remains a challenge. Since lyotropic systems offer a facile route to reaching analogous LC phases, the study of lyotropic systems and their behaviour may offer a way to achieve this goal.

While use of lyotropic systems bypasses many of the problems associated with thermotropic systems of azobenzene, it introduces a few complexities such as solubility issues and solvent volatility. For these reasons it is of interest to understand the self-assembly of azobenzene molecules in a variety of solvents, and in particular solvents with high boiling points. Ionic liquids (ILs) are particularly of interest as solvents for simple azobenzene tectons because of their tunable properties and low to negligible volatility at room temperature and pressure.[33] The protic ionic liquids ethylammonium formate (EAF) and propylammonium formate (PAF), as well as the molecular solvents dimethyl sulfoxide (DMSO) and *N,N*-dimethylformamide (DMF) will therefore be investigated in this study.

In this paper we aim to explore structure-function relationships

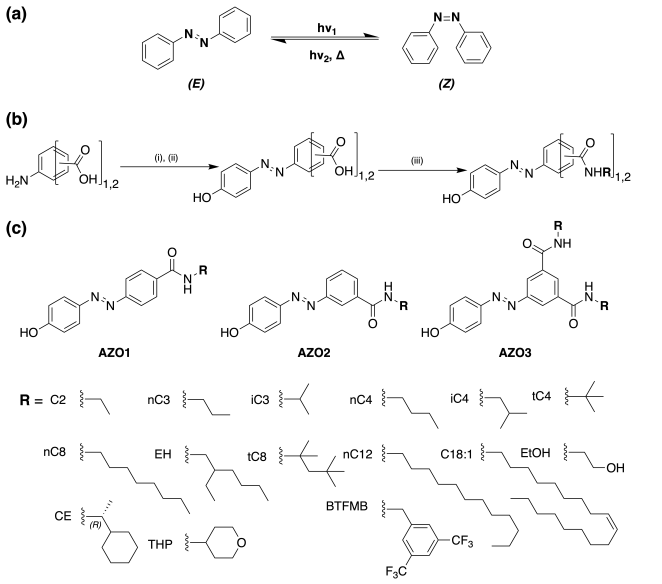

Fig. 1 (a) Isomerization of azobenzene. (b) Synthetic scheme for azobenzene-based molecules. (i) $NaNO_2$ (1.1 equiv.), HCl (xs.), H_2O, 0°C, 2h (ii) Phenol (1.1 equiv.), NaOH (0.7 equiv.), K_2CO_3 (0.7 equiv.), H_2O, 0°C - RT, 18h (iii) *N,N'*-Dicyclohexylcarbodiimide (DCC) (1.1 equiv.), *N*-hydroxysuccinimide (NHS) (cat.), $R-NH_2$ ($\geq$1.1 equiv.), DMF, RT, 18h (c) Library of azobenzene-based molecules and shorthand notations used throughout the paper.

that underly the formation of lyotropic LCs from simple azobenzene building blocks in protic ILs and high boiling point solvents. The identified systems and the structural relationships should offer insights for the development of other self-assembled systems of azobenzene-based materials and responsive LC materials.

2 Experimental methods

2.1 Materials

All materials purchased were $\geq$95% purity and used without further purification. 4-aminobenzoic acid, 3-amino-benzoic acid, 3,5-diaminobenzoic acid, phenol, sodium nitrite, *N,N'*-dicyclohexylcarbodiimide (DCC), formic acid and all amines were purchcased from Sigma Aldrich, with the exception of 4-aminotetrahydropyran which was purchased from Combi-blocks. Deuterated solvents, D_2O and DMSO-*d6*, were purchased from Cambridge Isotope Laboratories Inc. The protic ionic liquids ethylammonium formate (EAF) and propylammonium formate (PAF) were synthesized by mixing stoichiometric quantities of formic acid with ethylamine (70% in water) or propylamine (neat) before drying under vacuum until constant mass.

2.2 Synthesis of azobenzene library

The library of simple azobenzene molecules was synthesized using a two step procedure of azo-coupling phenol to the relevant aminobenzoic acid, and subsequent DCC coupling of various amines to the pendant benzoic acid groups (Figure 1b). This synthetic route was based on the synthesis of similar molecules.[34–40] Full details of the synthesis and molecular characterizations are given in the ESI.†

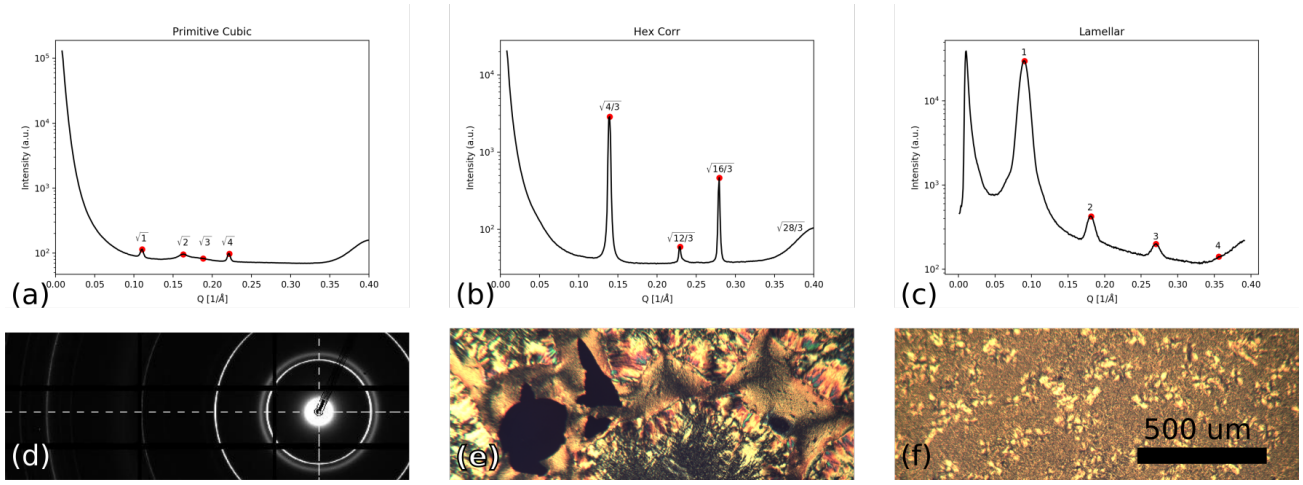

Fig. 2 Examples of mesophase identification from SAS patterns and representative PLM. (a) Representative peak identification for a primitive cubic mesophase. SAS pattern has a restricted q-range for clarity. (b) Representative peak identification for a hexagonal micellar ($P6_3mmc$) mesophase. SAS pattern has a restricted q-range for clarity. (c) Representative peak identification for a lamellar mesophase. (d) A representative 2D detector image from the synchrotron SAXS before reduction to a 1D pattern. Note that the beam-stop is visible in the detector image as a black shadow. (e) Representative PLM image for a hexagonal micellar ($P6_3mmc$) mesophase. (f) Representative PLM image for a lamellar mesophase.

The library of azobenzene molecules is given a shortened notation to reflect both the azobenzene core group and the amide substitution. The azobenzene core is noted numerically: the *para*-substituted 4-(4(hydroxyphenyl)diazenyl)benzoic acid core is denoted AZO1, the mono-*meta*-substituted 3-(4(hydroxyphenyl)diazenyl)benzoic acid core is denoted AZO2, and the di-*meta*-substituted 5-(4(hydroxyphenyl)diazenyl)isophthalic acid core is denoted AZO3. The *R*-group substitution is noted after the core group where the alkyl substitutions are noted with the number of carbon molecules and prefixed with the isomeric form (where applicable); unsaturated alkyl chains are noted by the number of carbons followed by the number of unsaturations. For *R*-groups that do not fit the aforementioned trend, the 2-hydroxyethyl substitution is shortened to EtOH, 4-tetrahydropyran to THP, (*R*)-1-cyclohexylethyl to CE, 2-ethylhexyl to EH and 3,5-bistrifluoromethylbenzyl to BTFMB. The library of azobenzene-based molecules is displayed in Figure 1c.

2.3 Small-angle scattering (SAS)

2.3.1 Small and wide-angle X-ray scattering (SAXS/WAXS).

Small-angle X-ray scattering (SAXS) measurements were obtained using the SAXS/WAXS beamline at the Australian Synchrotron, Clayton, Australia, using incident X-ray radiation with $\lambda = 1.0322$ Å (12 keV beam) and a Bruker NanoSTAR II SAXS (Bruker AXS, Karlsruhe) using Cu-Kα radiation, $\lambda = 1.5418$ Å (45 kV, 110 mA), at ACNS, Lucas Heights, Australia. A detailed explanation of the experimental set-up from the SAXS/WAXS experiment at the Australian Synchrotron is given in the ESI.†

2.3.2 Small-angle neutron scattering (SANS).

Small-angle neutron scattering (SANS) measurements were obtained using the BILBY beam-line in time-of-flight mode with an asymmetric detector array at the Australian Centre for Neutron Scattering (ACNS), ANSTO, Lucas Heights, NSW.[41,42] Samples were prepared in 2 mm path-length demountable quartz cells. Contrast was induced by using deuterated solvents. Partially deuterated versions of the ionic liquids, EAF-*d3* and PAF-*d3* were produced by hydrogen exchange of the labile hydrogens from the amine functional groups in the ILs with D_2O. Samples of the ILs were subjected to two cycles of mixing with D_2O and drying to constant mass under vacuum immediately before preparation of the SANS samples.

2.3.3 Small-angle scattering (SAS) data handling.

All small-angle scattering spectra were converted from raw counts to 1D spectra of intensity, I, as a function of scattering vector, q, defined as:

$$q = \frac{4\pi}{\lambda} \sin \frac{\theta}{2} \quad (1)$$

where λ is the incident X-ray wavelength or neutron de Broglie wavelength and θ is the scattering angle.

Spacing as indicated by peak position, d, can be calculated using the equation:

$$d = \frac{2\pi}{q} \quad (2)$$

where d is the distance (*e.g.* the interlamellar spacing for a lamellar mesophase).

Reduction of SAXS/WAXS data from the Australian Synchrotron was done using the Scatterbrain program. Reduction of SANS data from the BILBY beam-line was done using standard BILBY methods.

2.4 Polarising light microscopy (PLM)

Polarising light microscopy (PLM) photomicrographs were obtained using a CCD camera (Flea3, Point Grey, Richmond, BC, Canada) coupled to a polarizing light microscope (Kozo XJP 300 or Nikon Ci-S). Temperature control was achieved using a peltier

temperature stage (Linkam Scientific PE120) coupled to a recirculating water bath, with an accuracy of $\pm 0.1^{\circ}$C.

2.5 Photo-isomerization of samples

Photo-isomerization of the azobenzene LC samples was achieved using a 365 nm LED light source with 3 mW cm^{-2} incident light intensity. PLM samples were switched *in situ*. SANS and SAXS samples were isomerized off-line for 20 minutes unless otherwise stated, and protected from further external light exposure using aluminium foil shielding. Aluminium shielding was removed from SAXS samples before scattering patterns were recorded whereas SANS samples were left covered because of the transparency of the aluminium foil to the incident neutron beam and the long waiting times for scattering patterns to be obtained. Brief schematics for the isomerization set-ups are provided in the ESI.†

3 Results and Discussion

Lyotropic liquid crystal (LC) mesophases were formed from binary (azobenzene + solvent) mixtures of the library of simple azobenzene molecules listed in Figure 1 with the protic ionic liquid (IL) solvents EAF and PAF or the high boiling point solvents DMSO and DMF. The structural characteristics of the LC mesophases formed were investigated using small-angle scattering (SAS) and polarizing light microscopy (PLM) methods, and the results of these investigations are described in the following sections.

3.1 Mesophase identification

To identify LC mesophases using small-angle scattering, the radially averaged SAS patterns had their peaks indexed and matched to corresponding peak indices for the most likely mesophase peak positions. Some examples of mesophase identification from SAS patterns are given in Figure 2. A complete set of the raw 1D scattering patterns are given in the ESI.†

A complete list of identified LC phases and key spacing parameters from the SAS analysis are listed in Table 1. The molecules have been grouped by their core azobenzene unit (AZO1, AZO2 or AZO3) with increasing *R*-group length down the table. The substitutions that do not easily fit into this trend (R = EtOH, THP, (*R*)CE and BTFMB) are placed after the main alkyl series.

Where concentration dependent phase behaviour was identified the binary (azobenzene + solvent) systems were generally seen to follow the typical lyotropic transitions of Micellar (M) $\rightarrow$ Cubic (Q) $\rightarrow$ Hexagonal $\rightarrow$ Lamellar (L_α).

Phase identification in scattering patterns where multiple mesophases coexist was done by identifying peak correlation across concentration changes in the sample. Crystalline space groups, identified by their characteristically sharp Bragg peaks and typical space group parameters below 20 Å are not considered of interest for this study and have been ignored.

3.2 Structural trends

In the following section several trends from the identified mesophases and their relationships with the azobenzene tecton structure will be explored. Structural isomeric *R*-groups will be contrasted depicting effects of steric bulk on LC mesophase formation. Alkyl-group substitutions and their control over phase spacing are considered. Finally, position of the substitution on the azobenzene aromatic ring and the implication this has for preferencing specific mesophases is explored.

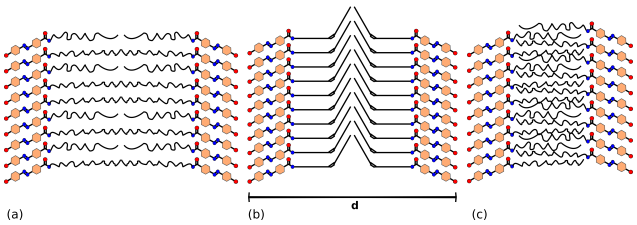

Fig. 3 Arrangements of molecules in lamellar bilayers. (a) fluid lamellar, L_α (b) lamellar gel phase, L_β (c) interdigitated packing. *d* indicates the inter-lamellar sheet distance in the bilayer structure.

3.2.1 Control of LC formation by *R*-group branching.

The library of azobenzene molecules included three sequences of *R*-group substitutions, demonstrating changes in the branching on the behaviour of the self-assembly of the systems; propyl (*n, i*), butyl (*n, i, t*) and octyl (*n, t* and 2-ethylhexyl (EH)). The two primary differences in the function of the *R*-group caused by increased branching are the change in the length and shape of the substituted group (with the branched groups decreasing in length and increasing in steric bulk around the branch points), and the decrease in the flexibility of the group caused by the changes in the structural isomeric form.

Changes to *R*-group branching are anticipated to have a two-fold influence on formation of LC mesophases: changes in the shape of the *R*-group substitution will influence the preferred packing arrangement of molecules in the mesophase, whereas decreases in flexibility caused by branching of the substituted group may influence the likelihood of liquid oil-like tail-group interactions. Therefore unbranched versions should have a greater likelihood of LC mesophase formation rather than a rapid transition from crystalline solid to molecular solution.

The second of these influences is noted in the number of LC mesophases identified for unbranched substitutions in comparison to their isomeric branched *R*-groups. This is particularly true for short chain lengths, with the *i*-propyl substitution displaying nearly no LC formation in comparison to the unbranched *n*-propyl. From these findings it can be suggested that branching can be utilised for the control of self-assembled packing only in longer substitutions where diverse mesophase behaviour is present.

3.2.2 Liquid crystal (LC) mesophase spacing trends.

The prevalence of lamellar phase throughout analysed binary mixtures make it ideal for comparison of spacings within self-assembled structures. Figure 4a compares the inter-sheet *d*-spacing (see Figure 3) of identified lamellar phases with the number of carbons in the longest unbroken chain in the *n* and

Table 1 Identified liquid crystalline phases and key spacing parameters

Molecule	EAF	PAF	DMSO	DMF
AZO1-C2[b]	Prim(31.5Å)	-	-	-
AZO1-*n*C3	Ia$\bar{3}$d(29.1Å), L(34.8ÃĚ)	Ia$\bar{3}$d(29.1Å), Prim(34.1Å)	L(21.7Å)	L(21.8Å)
	L(30.9Å)	**-**	**-**	**-**
AZO1-*i*C3[b]	L(32.8Å)	-	-	-
AZO1-*n*C4	L(34.7Å)	L(34.7Å)	-	L(21.8Å)
	L(35.2Å)	**L(34.7Å)**	**-**	**L(21.9Å)**
AZO1-*i*C4	Ia$\bar{3}$d(28.9Å), L(30.5Å)	L(67.3Å)	-	-
	L(30.5Å)	**-**	**-**	**-**
AZO1-*t*C4	-	-	L(21.8Å)	L(21.9Å)
	-	**-**	**L(22.4Å)**	**L(21.9Å)**
AZO1-*n*C8	P6$_3$mmc(52.6Å)	P6$_3$mmc(52.7Å)	-	-
	P6$_3$mmc(52.9Å)	**P6$_3$mmc(52.4Å)**	**-**	**-**
AZO1-*t*C8	P6$_3$mmc(44.5Å)	-	-	[a]
	Prim(35.5Å)	**-**	**-**	**[a]**
AZO1-EH[b]	-	Ia$\bar{3}$d(27.8Å)	-	P6$_3$mmc(54.1Å), L(50.1Å)
AZO1-*n*C12	L(54.4Å)	L(53.6Å)	Prim(64.1Å), L(53.8Å)	Prim(53.5Å), L(53.8Å, 59.3Å)
	Prim(54.7Å), L(54.7Å)	**L(53.6Å)**	**Pn$\bar{3}$m(25.1Å), L(59.5Å)**	**Prim(20.4Å)**
AZO1-C18:1	L(67Å, 92Å)	L(67Å, 93Å)	M, Prim(69Å), P6$_3$mmc(81Å),	[a]
	L(67Å, 92Å)	**L(67Å, 93Å)**	L(72Å, 63Å) **M, Prim(69Å), P6$_3$mmc(81Å),**[c] **L(72Å, 63Å)**	**[a]**
AZO1-EtOH	L(23.1Å)	-	L(21.8Å)	L(21.8Å)
	L(22.8Å)	**-**	**L(21.9Å)**	**L(21.9Å)**
AZO1-THP	L(64.3Å)	L(63.1Å)	P6$_3$mmc(25.0Å), Ia$\bar{3}$d(30.2Å),	L(21.8Å)
	L(64.2Å)	**L(62.6Å)**	L(40.0Å) **P6$_3$mmc(25.0Å), Ia$\bar{3}$d(30.2Å), L(40.0Å)**	**L(21.8Å)**
AZO1-(*R*)CE	P6$_3$mmc(58.1Å)	Pn$\bar{3}$m(67.4Å)	-	-
	L(47.7Å)	**Pn$\bar{3}$m(67.4Å)**	**-**	**M**
AZO1-BTFMB[b]	-	-	-	P6$_3$mmc(25.9Å)
AZO2-C2[b]	-	Pm$\bar{3}$n(43.1Å), Fd$\bar{3}$m(22.2Å)	-	-
AZO2-*n*C3[b]	Pm$\bar{3}$n(20.7Å)	Pm$\bar{3}$n(21.9Å)	Pn$\bar{3}$m(20.5Å, 40.6Å)	-
AZO2-*i*C3[b]	-	-	-	-
AZO2-*n*C4[b]	Pm$\bar{3}$n(22.7Å)	Prim(20.7Å), Pm$\bar{3}$n(69.1Å)	L(47.6Å)	-
AZO2-*i*C4[b]	Pm$\bar{3}$n(23.5Å)	Pm$\bar{3}$n(23.5Å)	-	-
AZO2-*t*C4[b]	-	-	L(49.6Å)	L(49.6Å)
AZO2-*n*C8[b]	L(49.0Å)	L(23.5Å, 48.5Å)	L(23.5Å, 48.5Å)	Pn$\bar{3}$m(21.0Å), L(48.5Å)
AZO2-*t*C8[b]	-	P6$_3$mmc(55.3Å)	Pn$\bar{3}$m(68.4Å)	Pn$\bar{3}$m(63.9Å)
AZO2-EH[b]	P6$_3$mmc(66.5Å)	Pn$\bar{3}$m(20.6Å)	-	-
AZO2-*n*C12	[a]	Pn$\bar{3}$m(59.8Å), P6$_3$mmc(43.1Å), L(42.3Å)	Ia$\bar{3}$d(92.3Å)	M
	Pn$\bar{3}$m(63.8Å)	**Pn$\bar{3}$m(64.2Å), L(21.7Å)**	**Ia$\bar{3}$d(92.6Å)**	**-**
AZO2-C18:1	L(45.3Å)	L(45.5Å)	L(45.4Å)	Pn$\bar{3}$m(64.0Å), L(45.4Å)
	L(45.4Å)	**M, L(45.5Å)**	**-**	**M, L(44.9Å)**
AZO2-EtOH[b]	-	-	-	-
AZO2-THP[b]	-	M, P6$_3$mmc(23.1Å)	P6$_3$mmc(20.1Å), L(39.7Å)	P6$_3$mmc(20.0Å), L(39.9Å)
AZO2-(*R*)CE[b]	Pm$\bar{3}$n(22.5Å)	-	P6$_3$mmc(20.1Å)	-
AZO2-BTFMB [b]	-	-	-	Pn$\bar{3}$m(21.0Å)
AZO3-C2[b]	Pm$\bar{3}$n(24.6Å)	-	-	-
AZO3-*n*C3[b]	-	-	-	Pn$\bar{3}$m(20.1Å)
AZO3-*i*C3[b]	-	-	-	Pn$\bar{3}$m(20.1Å)
AZO3-*n*C4[b]	-	-	Pn$\bar{3}$m(20.1Å)	Pn$\bar{3}$m(20.1Å)
AZO3-*i*C4[b]	-	-	-	Pn$\bar{3}$m(20.5Å)
AZO3-*t*C4[b]	-	-	-	-
AZO3-*n*C8[b]	P6$_3$mmc (30.7Å), L(24.8Å)	P6$_3$mmc (30.7Å), L(24.8Å)	L(24.8Å)	P6$_3$mmc (31.3Å), L(24.4Å)
AZO3-*t*C8[b]	-	-	-	-
AZO3-EH[b]	P4332(22.8Å)	-	-	-
AZO3-*n*C12	-	L(34.8Å)	L(34.7Å)	L(34.6Å)
	-	**L(35.0Å)**	**L(34.9Å)**	**L(34.7Å)**
AZO3-C18:1	-	L(45.2Å)	L(45.3Å)	L(45.5Å)
	-	**L(45.6Å)**	**L(45.5Å)**	**[b]**
AZO3-EtOH[b]	-	-	-	-
AZO3-THP[b]	M, P6$_3$mmc(24.9Å)	P6$_3$mmc(55.4Å), L(42.1Å)	M, P6$_3$mmc(55.4Å), L(42.1Å)	M
AZO3-(*R*)CE[b]	-	-	Ia$\bar{3}$d(32.6Å)	Ia$\bar{3}$d(32.5Å), P4332(21.2Å)
AZO3-BTFMB[b]	-	M	-	-

M – Micellar, L – Lamellar, P6$_3$mmc – Hexagonal micellar, - – No liquid crystalline phases identified, **Bold** – After 20 minutes of UV irradiation (365 nm), [a] – Sample conditions were not run, [b] – UV-switching not done, [c] – Partial disordering and loss of later correlation peaks (see Figure 5).

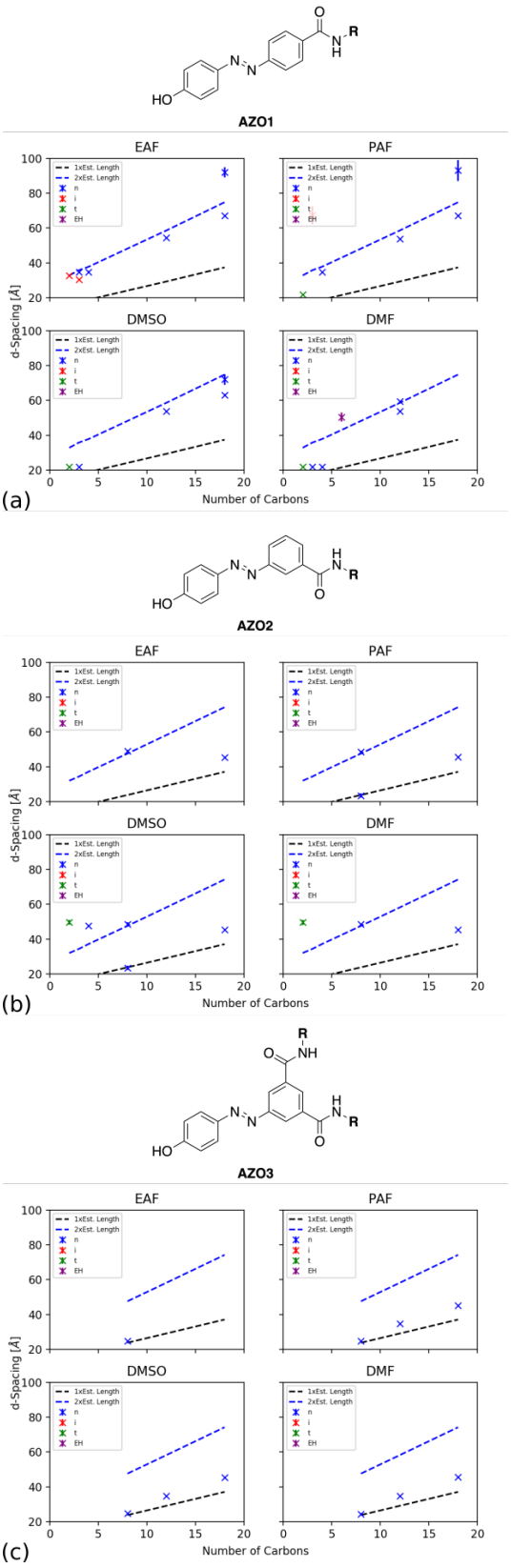

Fig. 4 The identified key spacings in the lamellar phases molecules with comparison the the number of carbons in the longest continuous chain in the straight and branched alkyl *R*-group substitutions. (a) AZO1 core-group. (b) AZO2 core-group. (c) AZO3 core-group.

branched-alkyl *R*-substitutions on the *para* substituted azobenzene (AZO1). These results indicate a positive trend in the inter-lamellar sheet spacing in all solvent systems.

The molecular length of the azobenzene library was estimated by comparing the distance between the oxygen on the phenolic functional group to the furthest carbon atom in the variable *R*-group using ChemDraw Professional. More information on estimated molecular lengths are given in the ESI†. Though the occurrence of multiple identified lamellar spacings confounds identification of a specific trend, the occurrence of larger phase spacings could be due to initiation of phase separation or, especially in the case of R = C18:1 samples, differences in the tilt of the tail-group packing (L_α *vs* L_β) (see Figure 3). When compared to estimated molecular lengths, lamellar spacings roughly correspond to twice the length of the respective molecules. This indicates that the lamellar sheets are composed of an azobenzene bilayer. It is noted that there is a slight divergence from idealized length, especially for long *R*-groups and groups with branching. This observed effect can be considered as an effect of the packing of azobenzene molecules in the bilayer structure.

Similar comparisons for the two other core-groups, the mono-*meta*-substituted AZO2, and the di-*meta*-substituted AZO3, are given in Figure 4b and c respectively. It is noted that AZO2 compounds lack a positive trend in lamellar spacing contrary to both AZO1 and AZO3 samples. AZO3 samples display a similar positive trend to AZO1 samples, though with a noted smaller spacing of the lamellar phase for similar continuous chain lengths. The protic IL EAF only displays one lamellar phase, likely caused by insolubility of the multiple large lipidic *R*-group functionalities without greater compensation by a polar functionality.

Inter-lamellar spacings for AZO3 samples were found to roughly compare to the estimated length of a single molecule, whereas AZO1 samples more closely resembled twice the estimated molecular lengths. Where AZO1 bilayers likely displayed very little interdigitation of the variable *R*-groups, the two substitutions from the AZO3 core-group favour this closer packing arrangement.

Trends for all core-groups and solvent combinations are dominantly controlled by core and *R*-group substitution without much influence from solvent choice after minimum solubility requirements are met. Lamellar phase spacings can be predictably controlled by extending the length of the *R*-group substitution to control bilayer spacing, especially in linear AZO1 samples where very little tail-group interdigitation was observed. Where bends in the molecular structure or multiple substitutions are present, more complex packing arrangements need to be considered.

3.2.3 Mesophase prevalence control by core-group.

Comparing the frequency of occurrence of various mesophases formed by changing the substitution position on the azobenzene core group, a strong preference for cubic mesophases in the *meta*-substituted AZO2 is identified. Table 2 indicates the frequency of various mesophases by azobenzene core-group. The major change noted between samples is the prevalence of cubic phase especially in comparison to lamellar phase. The frequency of occurrence of hexagonal phase does not shift as dramatically across

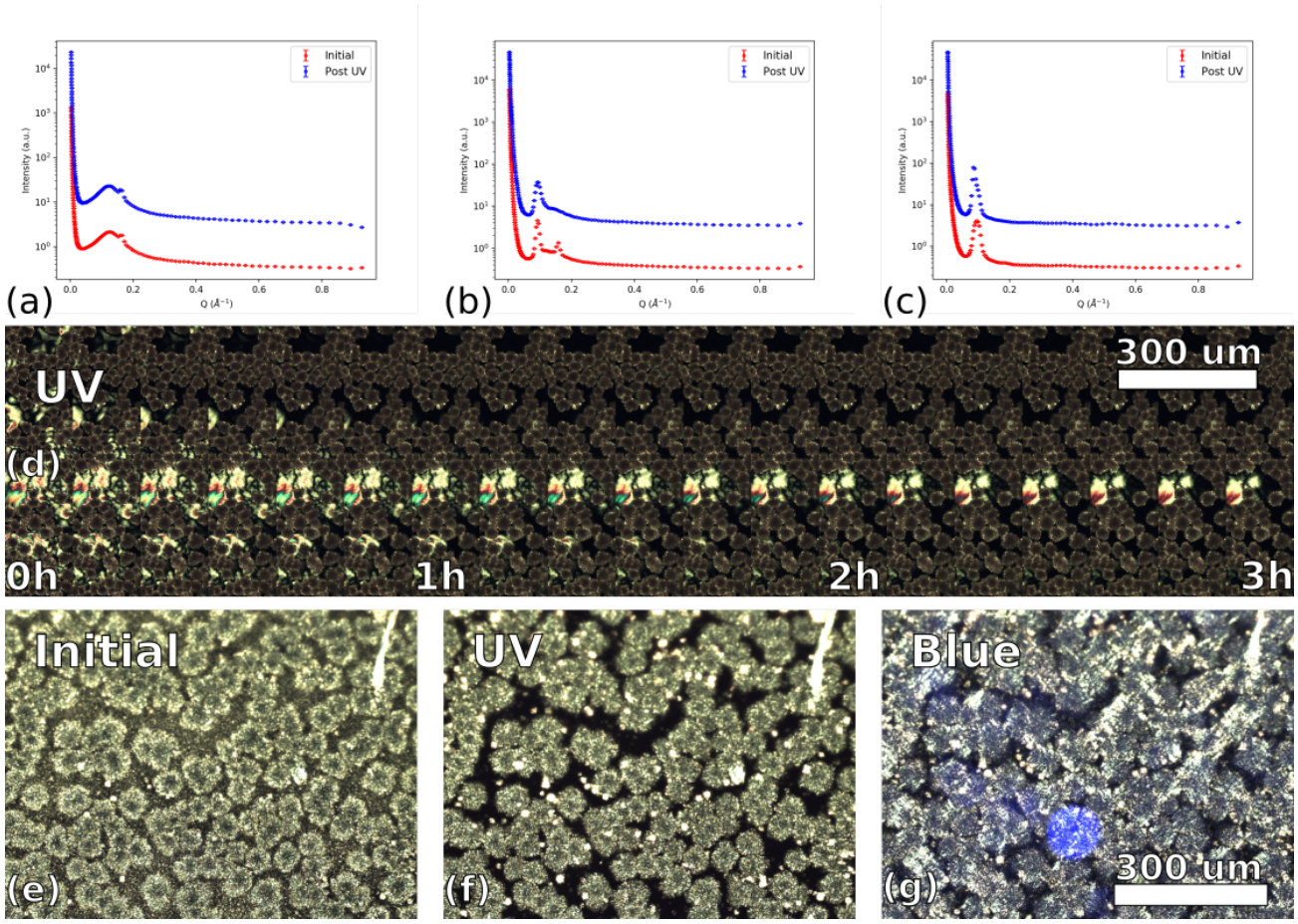

Fig. 5 (a) SANS scattering pattern of 55 wt. % AZO1-C18:1 in DMSO before and after 30 minutes of 365 nm UV irradiation. (b) SANS scattering pattern of 75 wt. % AZO1-C18:1 in DMSO before and after 60 minutes of 365 nm UV irradiation. (c) SANS scattering pattern of 95 wt. % AZO1-C18:1 in DMSO before and after 30 minutes of 365 nm UV irradiation. (d) PLM image of the *in situ* photo-isomerisation of 80 wt. % C18:1 in DMSO (100× magnification). (e) PLM image of 80 wt. % C18:1 in DMSO before isomerization (100× magnification). (f) PLM image of 80 wt. % C18:1 in DMSO after UV isomerization (100× magnification). (g) PLM image of 80 wt. % C18:1 in DMSO after blue light back-isomerization (100× magnification).

the varied core-group substitutions. Both mono and di-*meta*-substituted AZO2 and AZO3 show a greater preference for cubic mesophase formation than the linear *para*-substituted AZO1, though the strongest preference is noted in AZO2 samples with 46.5% of all identified mesophases being cubic.

Samples can also be compared by the type of cubic space-group formed. A tally of cubic space-groups is given in Table 3. Similar to the preferences noted for formation of cubic phases, the difference in the most common space-groups is most stark comparing *para* AZO1 samples to mono-*meta* AZO2 samples. Where *para* substitution (AZO1) nearly exclusively produces primitive and Ia$\bar{3}$d space groups, AZO2 samples strongly favour Pn$\bar{3}$m and Pm$\bar{3}$n. The AZO3 core-group shows a greater spread of space-groups identified, though there may be a preference for the Pn$\bar{3}$m space-group similar to the AZO2 core-group.

From these results it is apparent that changing the substitution position on the azobenzene core-group offers a simple way to rationally design specific mesophase preference. The bend introduced from *meta* substitution clearly offers a strong influence on the self-assembly of LC mesophases.

Table 2 Frequency of identified mesophases from predominantly *trans* samples

	Cubic (*Q*)	P6$_3$mmc (*Hex*)	Lamellar (L_α)	Total
AZO1	11 (22.5%)	8 (16.3%)	30 (61.2%)	49 (100%)
AZO2	20 (46.5%)	7 (16.3%)	16 (37.2%)	43 (100%)
AZO3	10 (35.7%)	6 (21.4%)	12 (42.9%)	28 (100%)

Table 3 Frequency of identified cubic mesophases from predominantly *trans* samples

	Prim/Other	Ia3d	Pn3m	Pm3n	Total
AZO1	5 (45.5%)	5 (45.5%)	1 (9.0%)	0 (0%)	11 (100%)
AZO2	2[a] (10%)	1 (5%)	9 (45%)	8 (40%)	20 (100%)
AZO3	2[b] (20%)	2 (20%)	5 (50%)	1 (10%)	10 (100%)

[a] Includes one occurrence of the Fd$\bar{3}$m space group in count, [b] Includes two occurrences of the P4332 space group in count.

3.3 Photo-switching

The effect of isomerization of the azobenzene core-group on LC mesophase formation in binary (azobenzene + solvent) mixtures was investigated by monitoring SAS patterns and PLM textures after irradiation with 365 nm light. The mesophases identified through SAXS peak indexing are noted in bold throughout

Table 1. Though many of the same mesophases are noted from mixtures before and after photo-isomerization, two effects are evident from switching: small shifts in critical spacing parameter of the mesophases and the disappearance of some mesophases after irradiation. Mesophases with non-zero curvature (cubic and hexagonal) appear to be particularly susceptible to disruption by isomerization.

Single concentrations of AZO1-C18:1 were investigated for photo-switching using SANS to identify the effect of isomerization on various LC mesophases. Figure 5a-c displays scattering patterns of AZO1-C18:1/DMSO mixtures before and after irradiation with 365 nm light. Isomerization was found to have little influence on already considerably disordered phases such as the micellar phase displayed in Figure 5a. Similarly, little effect was noted on the lamellar phase, Figure 5c, though a slight shift in the first correlation peak may be indicative of a slow change in inter-sheet spacing with an increased proportion of *cis* (*Z*) isomer present. The greatest effect was noted on the hexagonal phase (Figure 5b), in which slow disordering of the system was noted through loss of later correlation peaks after the initial Bragg peak, fitting with trends noted from the larger set of results from the library.

Shifts noted in lamellar phases upon irradiation in Table 1 as well as the shoulder formation on the initial correlation peak in Figure 5c are consistent with results expected from a change between L_β and L_α conformations. The multi-lamellar scattering lengths which were noted in particular for the AZO1-C18:1 series of samples matches previous results found from their coexistence.[43]

The dynamics of the AZO1-C18:1/DMSO system and effect of photo-isomerization on macroscopic birefringence properties of the hexagonal mesophase were explored using PLM. Slow disordering of the system shown by reduction in birefringence of the sample is shown in Figure 5d. The influence of blue light in restoration of the original birefringence is demonstrated in Figure 5e-g.

The slow rate of switching noted from these samples is likely to be influenced by a number of factors. The energy of molecular orbital transitions is known to be an important factor in the switching rate of azobenzene molecules, and adaptations with modified functional group substitutions could be designed for faster thermal switching.[44] Moreover, the investigated systems are optically dense, increasing the required time for noticeable effects from isomerization to be observed. Finally, isomerization in condensed systems such as surface absorbed monolayers (SAMs) has been shown to be noticably slower,[45] with curvature and decreased density of packing having an effect to make photo-switching more facile.[46,47] The most curved interface possible is found in microemulsions and previous studies have noted large macroscopic system changes possible from photo-switching in these systems.[48] This in tandem with self-assembly and packing of the molecules in the varied mesophases may help to explain why the effects of isomerization were more noticeable in mesophases with surface curvature.

4 Conclusions

A library of simple azobenzene-based molecules was investigated in terms of lyotropic liquid crystal (LC) behaviour in binary (azobenzene + solvent) mixtures employing the protic ionic liquids (ILs) ethylammonium formate (EAF) and propylammonium formate (PAF) as well as the high boiling point solvents dimethylsulfoxide (DMSO) and *N,N*-dimethylformamide (DMF). Minor structural changes in the azobenzene molecules provide simple guides for rational design of future responsive LC systems.

The length of the longest extended carbon chain in straight and branched alkyl substitutions offers a highly predictable way to influence the spacing of LC mesophases, especially for *para*-substituted AZO1 samples. This predictability was observed using one particular example of the lamellar phase to demonstrate changes in inter-lamellar sheet spacing due to its prevalence throughout binary mixtures.

Changes due to the influence of the core azobenzene group were also noted between the *para*-substituted AZO1, mono-*meta*-substituted AZO2 and di-*meta*-substituted AZO3. While a diverse array of mesophases were identified for all azobenzene core-groups the *meta*-substitution from the AZO2 series was shown to preference formation of cubic phases and particularly $Pn\bar{3}m$ and $Pm\bar{3}n$ space-groups compared to primitive and $Ia\bar{3}d$ cubic space-groups which were more common with the *para*-substituted AZO1 series.

Varying influence of isomerization was noted in the identified mesophases, with mesophases with non-zero curvature identified as more susceptible to disruption of self-assembled structure. Isomerization of lamellar mesophases, especially in liquid crystals formed by the AZO1-C18:1 molecule, displayed scattering patterns that may indicate a partial disruption of mesophase structure, such as a partial L_β to L_α transition, however, they maintained their overall lamellar structure. The ability of photo-isomerization to influence self-assembly of LC systems, especially disordering of hexagonal mesophases which is apparent in changes observed in macroscopic birefringence properties of the LC, indicating the potential of these, or similar systems, to be applied in optical devices.

The influences identified from simple changes to variable group length, substitution position and curvature of the self-assembled mesophase on photo-switching provide the means for rational design of specific systems for light-responsive materials in optical devices.

Conflicts of interest

There are no conflicts to declare.

Acknowledgements

We acknowledge the support of the ANSTO, in providing travel funding and access to the SAXS/WAXS beamline at the Australian Synchrotron, Melbourne, Australia, and access to BILBY and Bruker NanoStar II SAXS at the Australian Centre for Neutron Scattering (ACNS), Sydney, Australia, used in this work. The authors would like to thank AINSE Limited for providing financial assistance (Award - PGRA) to enable work on ANSTO beamline

facilities. This research was supported by an Australian Government Research Training Program (RTP) Scholarship.

References

1 E. K. Fleischmann and R. Zentel, *Angewandte Chemie - International Edition*, 2013, **52**, 8810–8827.

2 M. Schadt, *Mol. Cryst. Liq. Cryst.*, 2017, **647**, 253–268.

3 A. Sasaki, *Oyo Butsuri*, 1981, **50**, 1216–20.

4 T. Kato, J. Uchida, T. Ichikawa and T. Sakamoto, *Angewandte Chemie International Edition*, 2018, **57**, 4355–4371.

5 T. Kato, N. Mizoshita and K. Kishimoto, *Angewandte Chemie - International Edition*, 2005, **45**, 38–68.

6 J. P. F. Lagerwall and G. Scalia, *Current Applied Physics*, 2012, **12**, 1387–1412.

7 S. T. Hyde, Handbook of Applied Surface and Colloid Chemistry, pp. 299–332, 5 plates.

8 R. Yerushalmi, A. Scherz, M. E. Van Der Boom and H. B. Kraatz, *Journal of Materials Chemistry*, 2005, **15**, 4480–4487.

9 M. A. C. Stuart, W. T. S. Huck, J. Genzer, M. MÃijller, C. Ober, M. Stamm, G. B. Sukhorukov, I. Szleifer, V. V. Tsukruk, M. Urban, F. Winnik, S. Zauscher, I. Luzinov and S. Minko, *Nature Materials*, 2010, **9**, 101–113.

10 D. Roy, J. N. Cambre and B. S. Sumerlin, *Progress in Polymer Science (Oxford)*, 2010, **35**, 278–301.

11 H. Zhang, X. Meng and P. Li, *Progress in Chemistry*, 2008, **20**, 657–672.

12 Y. Zhao and T. Ikeda, *Smart Light-Responsive Materials: Azobenzene-Containing Polymers and Liquid Crystals*, 2008, pp. 1–514.

13 H. Xie, L. Wang, H. Wang, C. Zou, M. Wang, B. Wang, Z. Chen, L. Zhang, X. Zhang, Z. Yang and H. Yang, *Liquid Crystals*, 2015, **42**, 1698–1705.

14 E. Piosik, M. Kotkowiak, I. Korbecka, Z. Galewski and T. MartyÅĎski, *Physical Chemistry Chemical Physics*, 2017, **19**, 23386–23396.

15 Y. C. Liu, K. T. Cheng, Y. D. Chen and A. Y. G. Fuh, Proceedings of AM-FPD 2015 - 22nd International Workshop on Active-Matrix Flatpanel Displays and Devices: TFT Technologies and FPD Materials, pp. 69–72.

16 Y. H. Lin and M. S. Chen, 2016 Progress In Electromagnetics Research Symposium, PIERS 2016 - Proceedings, pp. 999–1002.

17 D. Ishikawa, E. Ito, M. Han and M. Hara, *Langmuir*, 2013, **29**, 4622–4631.

18 I. C. Khoo, *Physics Reports*, 2009, **471**, 221–267.

19 B. T. Hogan, E. Kovalska, M. F. Craciun and A. Baldycheva, *Journal of Materials Chemistry C*, 2017, **5**, 11185–11195.

20 P. Zhou, Y. Li, X. Li, S. Liu and Y. Su, *Liquid Crystals Reviews*, 2016, **4**, 83–100.

21 M.-M. Russew and S. Hecht, *Advanced Materials*, 2010, **22**, 3348–3360.

22 R. Yang, D. Zhao, G. Dong, Y. Liu and D. Wang, *Crystals*, 2018, **8**, 147.

23 S. A. A. Santos, W. C. Costa, I. H. Bechtold, R. A. P. Halfen, A. A. Merlo and L. F. Campo, *Liq. Cryst.*, 2019, **46**, 655–665.

24 X. Zhu, F. Yin, H. Zhao, S. Chen and Z. Bian, *RSC Adv.*, 2017, **7**, 46344–46353.

25 M. Alaasar, *Liquid Crystals*, 2016, **43**, 2208–2243.

26 Z. Miao, Y. Zhang, Y. Zhao, Z. Wang and D. Wang, *Molecular Crystals and Liquid Crystals*, 2014, **591**, 10–18.

27 A. R. Yuvaraj, M. Y. Mashitah and R. Lutfor, *Molecular Crystals and Liquid Crystals*, 2016, **631**, 21–30.

28 Z. C. Miao, Y. M. Zhang, Y. Z. Zhao and D. Wang, *Molecular Crystals and Liquid Crystals*, 2013, **582**, 98–106.

29 Y. C. Hsiao, K. C. Huang and W. Lee, *Optics Express*, 2017, **25**, 2687–2693.

30 S. W. Oh, J. M. Baek and T. H. Yoon, *Optics Express*, 2016, **24**, 26575–26582.

31 M. Wang, W. Hu, L. Wang, D.-Y. Guo, T.-H. Lin, L. Zhang and H. Yang, *Journal of Materials Chemistry C*, 2018, **6**, 7740–7744.

32 A. Nagai, H. Kondo, Y. Miwa, T. Kondo, S. Kutsumizu, Y. Yamamura and K. Saito, *Bull. Chem. Soc. Jpn.*, 2018, **91**, 1652–1659.

33 M. J. Earle, J. M. S. S. EsperanÃğa, M. A. Gilea, J. N. Canongia Lopes, L. P. N. Rebelo, J. W. Magee, K. R. Seddon and J. A. Widegren, *Nature*, 2006, **439**, 831–834.

34 E. O. Woolfolk and E. H. Roberts, *Journal of Organic Chemistry*, 1956, **21**, 436–438.

35 X. Pang, B. Xu, X. Qing, J. Wei and Y. Yu, *Macromolecular Rapid Communications*, 2018, **39**, 1700237.

36 X. Li, R. Wen, Y. Zhang, L. Zhu, B. Zhang and H. Zhang, *Journal of Materials Chemistry*, 2009, **19**, 236–245.

37 A. F. D. de Namor, R. Traboulssi and M. Salomon, *Journal of the Chemical Society, Faraday Transactions*, 1990, **86**, 501–505.

38 Z.-y. Li, H.-j. Quan, C.-b. Gong, Y.-z. Yang, Q. Tang, Y.-b. Wei, X.-b. Ma and H.-w. Lam, *Food Chemistry*, 2015, **172**, 56–62.

39 E. Valeur and M. Bradley, *Chemical Society Reviews*, 2009, **38**, 606–631.

40 E. Merino, *Chemical Society Reviews*, 2011, **40**, 3835–3853.

41 A. Sokolova, J. Christoforidis, A. Eltobaji, J. Barnes, F. Darmann, A. E. Whitten and L. de Campo, *Neutron News*, 2016, **27**, 9–13.

42 A. S. Tremsin, A. V. Sokolova, F. Salvemini, V. Luzin, A. Paradowska, O. Muransky, H. J. Kirkwood, B. Abbey, C. M. Wensrich and E. H. Kisi, *Rev Sci Instrum*, 2019, **90**, 035114.

43 D. Marquardt, F. A. Heberle, J. D. Nickels, G. Pabst and J. Katsaras, *Soft Matter*, 2015, **11**, 9055–9072.

44 J. GarcÃ■a-AmorÃşs and D. Velasco, *Beilstein journal of organic chemistry*, 2012, **8**, 1003–1017.

45 E. Titov, G. Granucci, J. P. GÃűtze, M. Persico and P. Saalfrank, *The Journal of Physical Chemistry Letters*, 2016, **7**, 3591–3596.

46 C. Liu, D. Zheng, W. Hu, Q. Zhu, Z. Tian, J. Zhao, Y. Zhu and J. Ma, *Nanoscale*, 2017, **9**, 16700–16710.

47 T. Moldt, D. Brete, D. Przyrembel, S. Das, J. R. Goldman, P. K. Kundu, C. Gahl, R. Klajn and M. Weinelt, *Langmuir*, 2015, **31**, 1048–1057.

48 R. F. Tabor, R. J. Oakley, J. Eastoe, C. F. J. Faul, I. Grillo and R. K. Heenan, *Soft Matter*, 2009, **5**, 78–80.